July 2021

Causes and Characteristics of Electrical Resistivity Variability in Shallow (<4 >m) Soils in Taylor Valley, East Antarctica

William S. Gutterman
Louisiana State University and Agricultural and Mechanical College

CAUSES AND CHARACTERISTICS OF ELECTRICAL RESISTIVITY VARIABILITY IN SHALLOW (<4 m) SOILS IN TAYOR VALLEY, EAST ANTARCTICA

A Thesis

Submitted to the Graduate Faculty of the
Louisiana State University and
Agricultural and Mechanical College
in partial fulfillment of the
requirements for the degree of
Master of Science

In

The Department of Geology and Geophysics

by
William Scott Gutterman
B.A., University of Colorado at Boulder, 2017

ACKNOWLEDGEMENTS

I am funded as a graduate assistant by the Louisiana State University Geology and Geophysics Department John Franks Fund. This research is funded by the National Science Foundation Grant #OPP-1637708 for the McMurdo Long Term Ecological Research site and #1643536 for Antarctic Airborne ElectroMagnetics (ANTAEM). I would like to give a special thanks to my graduate advisor, Peter Doran, for the immense support and guidance over the last 2 years and to my committee members, Juan Lorenzo and Carol Wilson, for their assistance along the way. Thank you to those that have provided crucial data and valuable discussions for this research including Krista Myers, Ross Virginia, Jeb Barrett, Mike Poage, Slawek Tulaczyk, Neil Foley, Jill Mikucki, Denys Grombacher, Hilary Dugan, and Esben Auken. Thank you to all MCM-LTER field team members for their support in the field and at home, specifically Michael Stone, Elizabeth Sicard, and Katie McNulty. Finally, I would like to thank my family and friends for encouraging me throughout this process and for being the bedrock of my success.

TABLE OF CONTENTS

ABSTRACT

The McMurdo Dry Valleys are the largest ice-free region in Antarctica and are characterized as a polar desert environment. Soils in the region are typically very dry (<1% soil water by weight) and remain frozen for most of the year. Increases in air temperature and incoming solar radiation during the austral summer generate meltwater from glaciers, ground ice, and snow patches supplying moisture to soils and altering the physical and chemical makeup of the subsurface. Previous studies have utilized airborne electromagnetic surveys (AEM) to analyze groundwater systems in the deep subsurface but have not yet examined soil moisture in the shallow (<4 m) subsurface. Here, I used electrical resistivity data from two AEM surveys (2011 and 2018) and soil geochemical data from three transects to characterize the spatial heterogeneity of soil properties in the near-subsurface of lower Taylor Valley. Soil resistivities from 2011 and 2018 range from 33.2 Ωm to 3535 Ωm with low elevations of <100 meters above sea level (masl) typically displaying the lowest resistivities and high elevations displaying greater resistivities. Liquid brine fractions were empirically estimated from electrical resistivity values using Archie's Law and range from 0.3% to 68.2% for soils with resistivities <200 Ωm. Additionally, soil transect data show greater percentages of fine-grained sediments (<63 μm) exist at elevations <100 masl where soil resistivities begin decreasing. Resistivity variability in the subsurface is ultimately controlled by the site history, local and regional climate, soil salinity, soil moisture, soil lithology.

INTRODUCTION

The McMurdo Dry Valleys (MDVs), situated along the coastal margin of Southern Victoria Land in East Antarctica, is a series of east-west trending valleys that make up the largest ice-free expanse in Antarctica (Levy, 2012). The region remains relatively ice-free due to the Transantarctic Mountains impeding the flow of the East Antarctic Ice Sheet (EAIS) into the area (Chinn, 1990). One of the largest valleys, Taylor Valley (TV), stretches ~50 km from the coast of the Ross Sea at McMurdo Sound to Taylor Glacier, an outlet glacier of the EAIS (Figure 1).

TV supports a hyperarid polar desert ecosystem, with maximum and minimum mean annual valley bottom temperatures ranging from -14.7°C to -23.0°C (Obryk et al., 2020), respectively, and annual precipitation varying from 3 to 50 mm water equivalent (Fountain et al., 2010). Low relative humidity and frequent strong wind events prompt high rates of sublimation with most snowfall sublimating before meltwater can infiltrate the subsurface (Chinn, 1993). Despite these regional climate conditions, melting of ice (glacier and lake) and snow occurs during the austral summer as air temperatures rise and incoming solar radiation increases significantly (Hoffman et al., 2016).

Landscape features in TV include alpine glaciers, ephemeral streams, perennially ice-covered lakes, and bare soils. Permafrost is continuous throughout the subsurface in TV and can be several hundred meters thick (McGinnis and Jensen, 1971; Mikucki et al., 2015). Soils in eastern TV are comprised mostly of glacial tills and fluviolacustrine deposits with ice-cemented permafrost dominating the near-surface (Bockheim et al., 2007). Active layers (seasonally thawed surface soils) form throughout the MDVs during the austral summer to depths of 0 to 75 cm (Bockheim et al., 2007), with the thickest

active layers forming near the coast (McGinnis and Jensen, 1971). The hydrology of the region is largely controlled by glacial stream discharge that delivers water, heat, and solutes to soils, stream margins, and lakes across the valley floor (Gooseff et al., 2011). In MDV soil ecosystems, the availability of liquid water is suggested as being the main limiting factor to life in these soil habitats (Gooseff et al., 2011).

Since 1992, research in the MDVs has been supported by the McMurdo Long-Term Ecological Research (MCM-LTER) project, which has focused most scientific efforts on studying ecological processes in TV. Soil development and distribution in TV has been thoroughly documented (Bockheim, 2002; Bockheim and McLeod, 2008; Campbell et al., 2013) and active layer processes in the top 1 m of the subsurface are well understood (Levy et al., 2011; Gooseff et al., 2013), however, there is a gap in knowledge on hydrological processes below this depth.

Airborne electromagnetic (AEM) methods have been used in the MDVs for detecting deep groundwater systems in TV (Mikucki et al., 2015; Foley et al., 2016, 2019) and provide insight into subsurface thermal regimes and geochemistry at greater depths. Basin-scale subsurface resistivity data collected in Fryxell Basin revealed an extensive zone of low resistivity, interpreted as liquid brine in sediments, stretching far beyond the surface expression of Lake Fryxell and extending several meters into the subsurface. Shallow soil (<4 m) properties including liquid water fraction and soil texture were characterized using electrical resistivity, soil-geochemical, meteorological, and satellite data, which improves our understanding of the hydrological, geochemical, and ecological processes occurring in the shallow subsurface and how these processes are affected by surface conditions in TV.

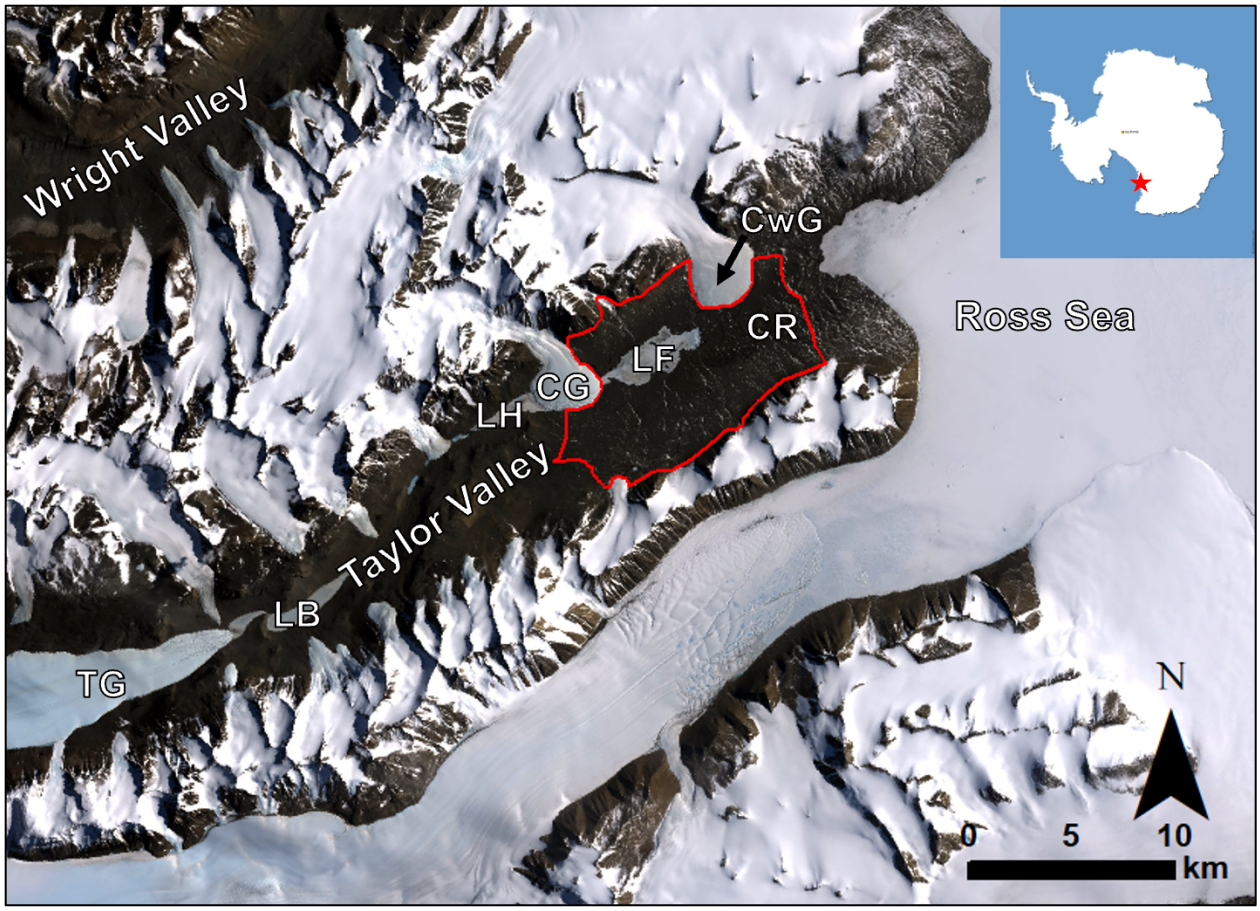

Figure 1. Overview map of Taylor Valley. Study area (Modified Fryxell Basin) shown with red line. The Eastern and Western boundaries follow drainage divides of Fryxell Basin excluding Canada and Commonwealth Glaciers, while the Northern and Southern limits roughly follow the 550 masl and 350 masl contours, respectively. CG = Canada Glacier, CwG = Commonwealth Glacier, LB = Lake Bonney, LF = Lake Fryxell, LH = Lake Hoare, RS = Ross Sea, TG = Taylor Glacier. Inset map shows location of the McMurdo Dry Valleys (red star). Satellite imagery from Landsat Imagery Mosaic of Antarctica (LIMA) modified from Bindschadler et al., (2017).

AIMS AND OBJECTIVES

This study aims to quantify the spatiotemporal distribution of wetted soils and the mechanisms controlling soil moisture accumulation in shallow porous materials in lower TV. Hydrological investigations of soils in the MDVs are typically limited to visibly saturated soils at shallow depths (<1 m), providing an opportunity to analyze and characterize soil-water dynamics at greater depths across an entire endorheic basin. Due to strict environmental regulations in the MDVs, geophysical techniques (e.g., AEM surveys) have recently become an effective method for examining the subsurface. Soil properties including soil texture, salinity, temperature, and degree of saturation can be estimated from AEM data. This study utilizes two separate AEM surveys from 2011 and 2018 as well as soil geochemical, meteorological, and satellite data to study the effect of surface conditions (i.e., soil characteristics, topography, and climate variability) on the accumulation and distribution of liquid water in the top 4 m of the subsurface of Fryxell Basin.

BACKGROUND

2.1. Hydrologic Setting in Taylor Valley

Lower Taylor Valley is a large relatively ice-free landscape within the MDVs that is occupied by perennially ice-covered Lake Fryxell, which lies between Canada Glacier and Commonwealth Glacier. The hydrology in Eastern Taylor Valley is largely controlled by the supply of meltwater from glacier, ground ice, and snow (Cartwright and Harris, 1981). Fryxell Basin is classified as an endorheic basin (no outflow). It comprises a watershed of 13 ephemeral streams that exchange glacial meltwater, salts, and nutrients with soils adjacent to lake margins and stream channels (Barrett et al., 2009; Cartwright and Harris, 1981; Gooseff et al., 2013; Toner and Sletten, 2013; Schmidt and Levy, 2017). The austral summer (November to February) is the only time streams are active as air temperatures and incoming shortwave radiation begin to increase, producing meltwater from local glaciers. Deltas form at locations where streams discharge into Lake Fryxell. Seasonally thawed soils form active layers in the subsurface during the austral summer that will undergo repeated freeze-thaw cycles as air and soil temperatures fluctuate (Wlostkowski et al., 2017).

2.2. Soil Distribution in Taylor Valley

The landscape of Eastern TV is characterized by large expanses of bare soils that encircle Lake Fryxell, a perennially ice-covered lake that lies between Canada and Commonwealth Glaciers. Soils in TV are often unconsolidated sediments that are coarsely grained with varying amounts of finer particles (Campbell et al., 2013). Sediment in eastern TV is characteristic of multiple glaciations (Prentice et al., 2013) and is primarily sourced from glacial tills of granitic origin with alluvium occurring on the valley floors

(Bockheim et al., 2007). Due to a lack of vegetation in the region, low soil organic matter contents are typical of TV soils. Maximum and minimum mean annual temperatures in lower TV are -16.9°C -23.0°C and there is a mean annual of 17 degree days above freezing (Obryk et al., 2020). Extremely cold mean annual temperatures cause soils in TV to remain frozen to depths of 200-600 m (Decker and Butcher, 1982), with a maximum annual average soil temperature at 0 cm depth of -16.4°C (Obryk et al., 2017). Soils sit above this continuous layer of permafrost, which is predominantly ice-cemented (cryoturbated) in lower TV, however dry-frozen permafrost (no cryoturbation) has been documented at high elevations on the Northern hillslopes above Lake Fryxell (Bockheim and McLeod, 2008). The spatial variability in permafrost form is due to heterogeneity in moisture sources and vapor pressure gradients (McKay et al., 1998), which relates to the different climatic zones (coastal, inland, or Polar Plateau adjacent) of the MDVs.

2.3. Geochemical Properties of Taylor Valley Soils

Electrical resistivity values of soils can be used as a proxy for salinity and provide insight into soil thermal regimes. Soil salinity in regions of continuous permafrost is largely influenced by ice/water content, texture, site history, and depth (Ugolini et al., 1981). When pore water freezes in soil, electrical resistivity values increase by several orders of magnitude (Mikucki et al., 2015). Based on AEM resistivity data, Mikucki et al. (2015) approximated resistivity ranges in Taylor Valley (Figure 2) for lake water (~0.1-30 Ωm), brine-saturated sediments (~10-800 Ωm), and permafrost/glacier ice (~500-20,000 Ωm).

Soil geochemistry in the MDVs is spatially heterogeneous and largely controlled by proximity to water sources and local climate conditions, such as precipitation and air

temperature (Wlostowski et al., 2017). The thermal properties of MDV soils are largely dependent on soil moisture content (Ikard et al., 2009), which typically decreases with

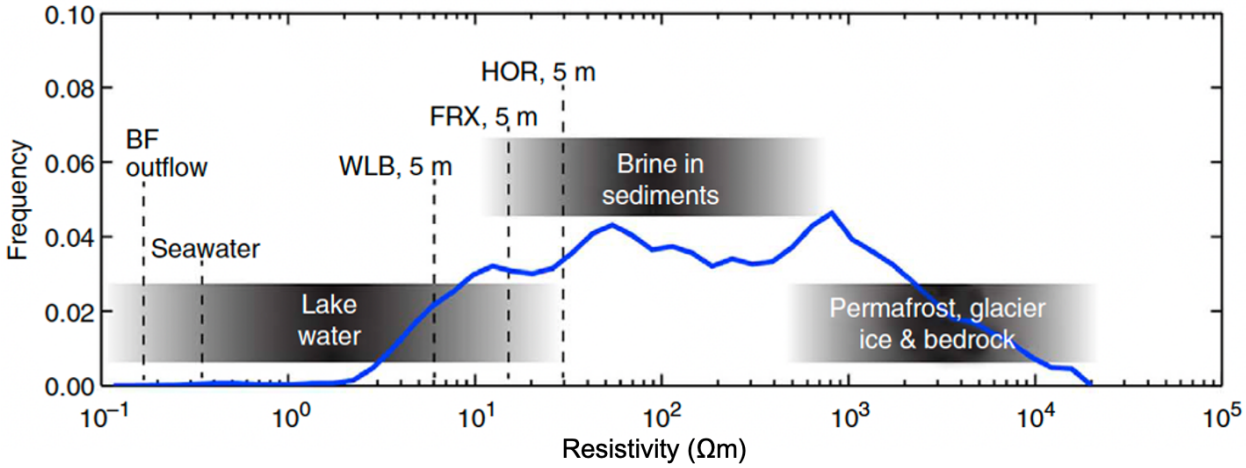

Figure 2. Relative frequencies and estimated resistivity ranges lake water, brine in sediments, permafrost, glacier ice, and bedrock from 2011 AEM survey within Taylor Valley are shown. The histogram was derived from the 2011 AEM data. Lower Taylor Valley in situ measurements marked: FRX, Lake Fryxell; HOR, Lake Hoare; WLB, West Lake Bonney (depth of measurement in meters follow abbreviation); BF, Blood Falls. Modified from Mikucki et al., (2015).

increasing distance from water sources. Wetted margins are sources of soil moisture found adjacent to streams and lakes and are caused by capillary wicking of moisture through porous spaces within soils (Gooseff et al., 2007). Soil moisture can also be sourced from snow patches, with some subnivian soils exhibiting moisture contents 20 times greater than adjacent exposed soils (Campbell et al., 2013; Gooseff et al., 2003). An additional water source is from spatially discrete wet patches that form next to drier soils. These wetted soil features form by deliquescence (i.e., atmospheric water vapor condenses into soil pore spaces) (Levy et al., 2014) and form water tracks (Levy et al., 2011). Water tracks route liquid water, sourced from snowmelt or melting ground ice, downhill above the ice table and exhibit very high solute concentrations. Valley bottom soils typically average ~1% water by volume in the upper 3 cm of the soil horizon

(Campbell et al., 2013), but moisture typically increases with increasing depth (Levy and Schmidt, 2016). Liquid water interacting with soils and sediments increases the fraction of total dissolved solids and releases ions, thus increasing the salinity of the substrate (Ugolini and Anderson, 1973).

A strong correlation exists between salinity and texture in MDV soils, with clays and silts displaying salinities up to 10 times greater than salinities in coarser sediments. Solutes in coarse sediments can be ‘flushed’ in hydrodynamic conditions, while clays and silts tend to retain solutes even as they interact with flowing water (Ugolini et al., 1981). TV soils are generally unconsolidated with coarse (sand) textures and smaller fractions of silt and clay (Campbell et al., 2013) sourced from granitic glacial tills and dolerite sandstones (Prentice et al., 2013). Differences in age and soil texture are responsible for variability in hydraulic conductivities between coastal and inland soils with less developed and younger coastal soils containing greater percentages of fine particles and displaying much greater hydraulic conductivities (Schmidt and Levy, 2017).

METHODS

3.1. SkyTEM Resistivity Surveys

SkyTEM, an AEM system utilizing time-domain electromagnetic (TDEM) sensors, was deployed in the MDVs in December of 2011 and November of 2018. A pulsed primary electromagnetic field was created using a large transmitter loop, which produced eddy currents in the ground and generated a secondary magnetic field (Figure 3). An induction receiver coil measured the time decay of the secondary electromagnetic field generated in the subsurface (Auken et al., 2009). Using the primary field decay equation, apparent conductivity can be calculated (Ward and Hohmann, 1988). In lower Taylor Valley, data coverage is much denser from the 2011 SkyTEM survey compared to the 2018 SkyTEM survey (Figure 4). SkyTEM survey dates within Fryxell Basin and the parameters used to generate resistivity maps are summarized in Table 1.

Table 1. SkyTEM Survey Information

AEM Survey Year	Flight Dates	# of Data Nodes	Node Spacing	Search Radius (m)	Interpolation
2011	Dec. 1-3 Dec. 5-6	8211	25	1000	Kriging
2018	Nov. 15 Nov. 26-27	706	50	250	Kriging

After data collection was completed, the raw resistivity data was processed and inverted using Workbench, a specialized inversion software developed by the University of Aarhus (Auken et al., 2009). A spatially constrained inversion scheme was used to create mean resistivity maps. Depth of investigation (DOI) is determined in Workbench and varies depending on subsurface characteristics. Lower DOIs (<100 m) are associated with low resistivity subsurface materials such as lake water and brine saturated sediments

(<1,000 Ωm) and higher DOIs (>300 m) are associated with high resistivity materials such as permafrost and glacier ice (>1,000 Ωm) (Mikucki et al., 2015; Foley et al., 2016).

Resistivity maps of the top 4 m were generated in Workbench using a 1,000 m search radius, 25 m node spacing, and kriging interpolation for the 2011 data. The 2018 resistivity maps also show the top 4 m and used kriging interpolation, but a 250 m search radius and 50 m node spacing were used. The smaller search radius was used for 2018 data to avoid over interpolation with such large gaps between flight lines and individual sounding points. The different node spacings used reflect the actual node spacing of the 2011 (25 m) and 2018 (50 m) datasets. Some flight line nodes were culled before generating resistivity maps to remove erroneous data.

The boundaries to the North and South of Lake Fryxell roughly follow the 550 masl and 350 masl contours, respectively. Canada Glacier and Commonwealth Glacier were excluded from the study area to focus the analysis on lower TV soils. The study area determined here is not a true representation of the entire Fryxell Basin and will be referred to, herein, as “Modified Fryxell Basin” (MFB). All AEM resistivity data reported in this study are from soils located within the boundaries of MFB. However, data within the boundaries of Lake Fryxell are not reported here apart from islands with soils sitting above lake level. Mean resistivity maps were exported from Workbench and imported into ArcGIS Pro to analyze the spatial variability in shallow soil resistivities. All data outside of MFB were clipped and data from Lake Fryxell’s waters were deleted to focus analysis on soils. A resistivity difference map was produced by subtracting 2011 resistivities from 2018 resistivities within MFB and where resistivity data overlapped. Additionally, elevations were extracted from the DEM to see how resistivity difference varied with elevation. To

further understand how topography affects groundwater accumulation and drainage density, Fryxell Basin surface slopes and aspects were determined from a 1 m/pixel airborne LiDAR digital elevation model (DEM; Fountain et al., 2017). Slopes and aspects were extracted to flight line nodes to determine if the degree of incline or orientation of the surface were important drivers of resistivity variability in the shallow subsurface.

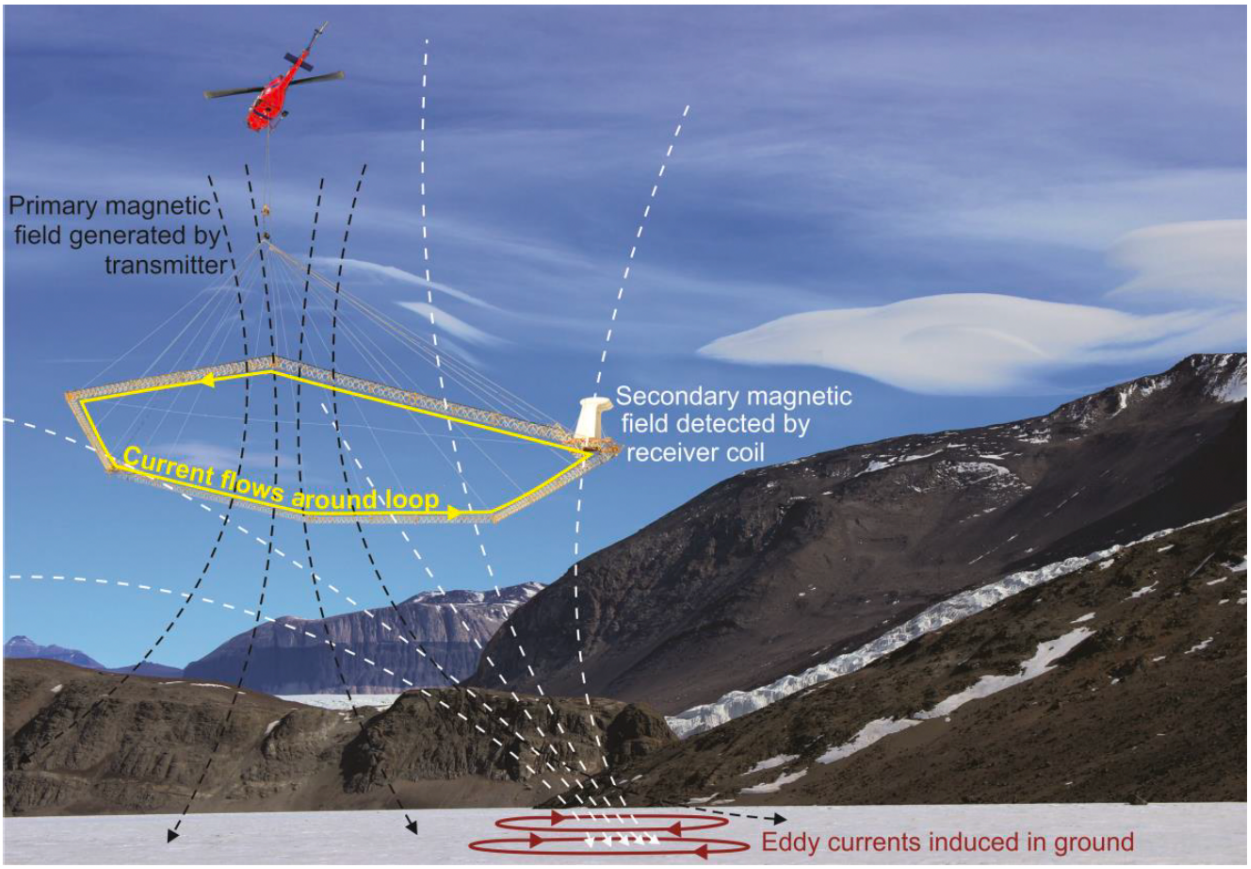

Figure 3. Schematic showing the SkyTEM time-domain electromagnetic (TDEM) system being flown over Lake Bonney in 2011. From Mikucki et al., (2015) supplemental information.

The relationship of resistivity to salinity, degree of saturation, porosity, and temperature allow for physical and chemical characteristics of the subsurface to be inferred (Mikucki et al., 2015). A threshold of ≤200 Ωm was used to delineate between unfrozen, partially saturated soils and frozen, dry soils. Regions with resistivity values of

200 Ωm to 500 Ωm are interpreted to be areas of degrading permafrost and resistivities >500 Ωm are inferred as completely frozen permafrost (ice-cemented and dry-cemented) (Mikucki et al., 2015). Resistivity values of saturated sediment determined during the Dry Valleys Drilling Project (McGinnis and Jensen, 1971) are similar to resistivity ranges used here. McGinnis and Jensen (1971) found saturated sands in Eastern Taylor Valley with resistivities ranging from 78 Ωm to >500,000 Ωm at temperatures of 21°C and -25°C, respectively, which suggests that 200 Ωm is a reasonable threshold for brine saturated sediments for this study.

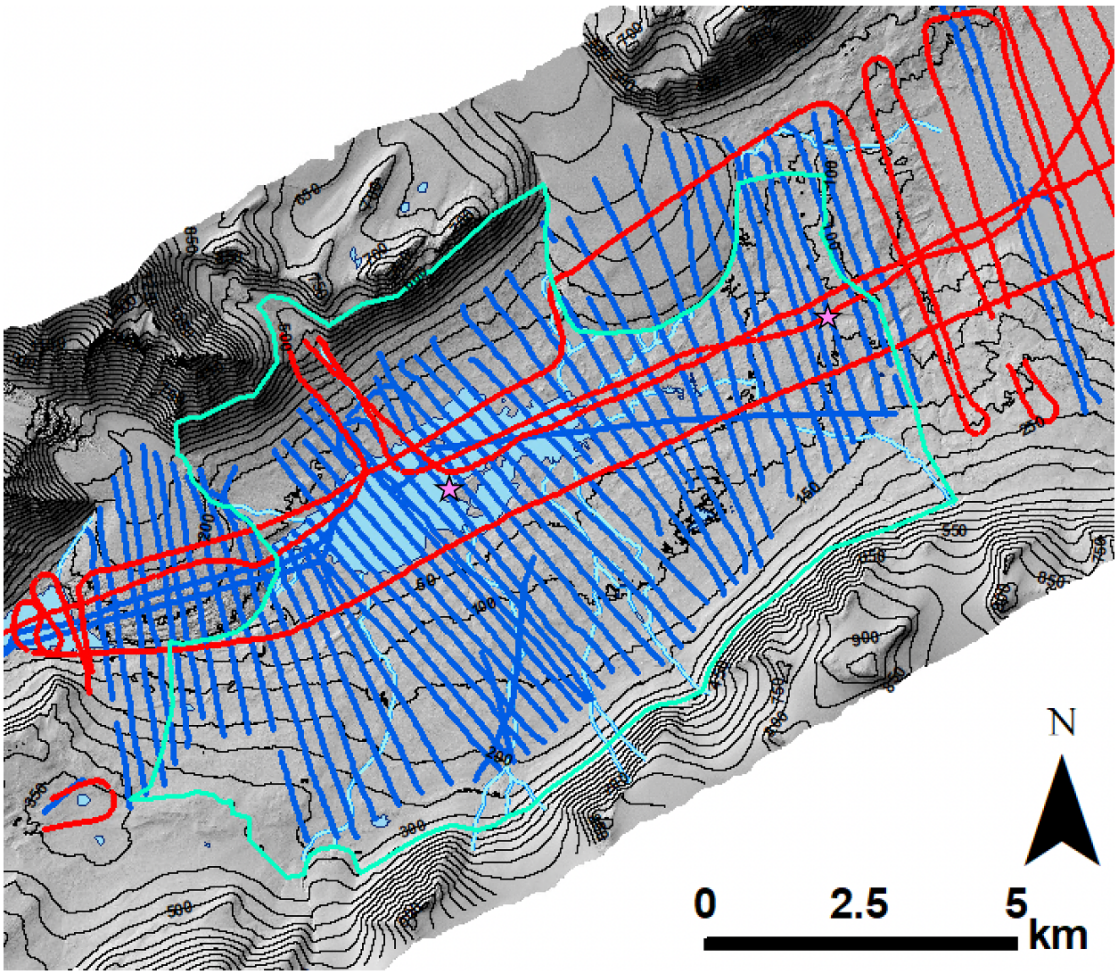

Figure 4. 2011 (blue) and 2018 (red) SkyTEM flight lines and study area (cyan) overlain on a shaded relief map derived from a DEM (1 m resolution) from 2014-15 LiDAR survey (Fountain et al., 2017). Lake Fryxell met station (FRLM; west) and Explorer's Cove met station (EXEM; east) shown with pink stars. Contour interval is 50 m.

Calculations of liquid brine fraction in sediments were done using Archie's Law (Archie, 1950), which relates the bulk resistivity of a formation to porosity. A simplified form of the equation is

$$\varphi = \left(\frac{\rho_0}{\rho_b}\right)^{-1/m} \quad \text{[Equation 1]}$$

where φ is the liquid brine fraction, ρ_0 is the bulk measured resistivity of the formation, ρ_b is the resistivity of the brine, and *m* is a cementation exponent that reflects properties of the pore network. The cementation exponent for unconsolidated sediments typically ranges from 1.1 to 1.6 (Archie, 1942; Frohlich and Parke; 1989; Byun et al., 2019). Resistivity of the actual brine is not known, so a range of soil moisture fractions were calculated using reasonable values for brine resistivities and cementation exponents. Archie's Law typically assumes the formation is fully saturated, but in this case the degree of saturation is unknown. Fully saturated conditions allow for porosity to be equated to water saturation; however, MDV soils typically exist in unsaturated conditions meaning porosity is not equal to soil moisture in this study. Here, Archie's Law calculations are reported as liquid brine fractions and do not represent the full volume of pore space. Unfrozen brine fraction estimations were then imported into ArcGIS and soil moisture maps were generated and overlaid on a 1 m/pixel resolution DEM (Fountain et al., 2017).

3.2. Soil-Geochemical Samples from Modified Fryxell Basin

Soil samples were collected along three transects (FRX-1, FRX-2, and FRX-3) within MFB to characterize soil properties at various elevations (Figure 5). The total distance of each transect is 3525 m (~280 m relief), 3740 m (~300 m relief), and 1546 m (~220 m relief) for FRX-1, FRX-2, and FRX-3, respectively. Samples from FRX-1 and

FRX-2 were collected on January 10, 2006, and FRX-3 samples were collected on December 21, 2007. A total of 528 samples were collected between FRX-1 (n = 218), FRX-2 (n = 182), and FRX-3 (n = 128). Individual soil samples (0-10 cm; ~150 g) were collected using individual aseptic plastic trowels and GPS positions of each sample were recorded. Estimations of soil-salinity were determined from measuring the conductivity of a 1:5 solution of the <2 mm size fraction in DI water using a calibrated Yellow Springs Instrument 3100 conductivity meter. Particle size analysis was performed on 46 soil sample subsets from FRX-1. Particle sizes were determined using a Coulter LS230 Particle Size Analyzer and are presented as the percent by mass of clay and silt (<63 μm) within the <2 mm size fraction. All geochemical and grain size analyses were done at Dartmouth University in either the Environmental Measurements Laboratory or the Stable Isotope Laboratory. Samples chosen for grain size analysis were selected so that the full length and range of elevations for the transect were represented.

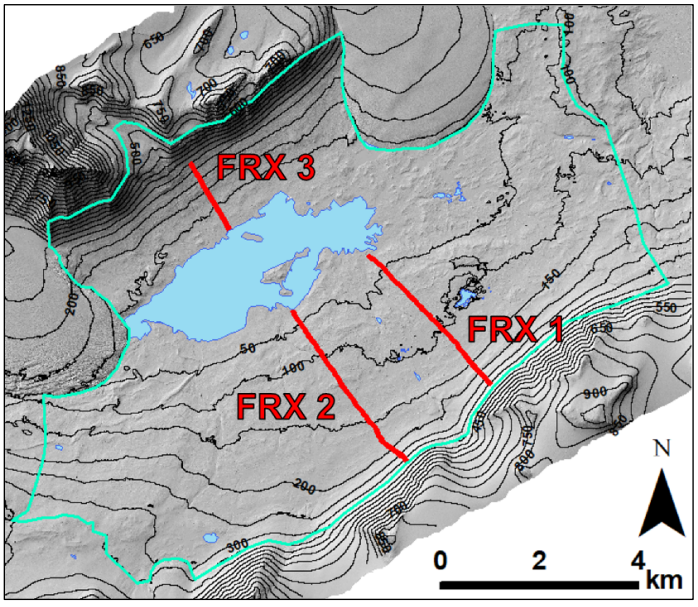

Figure 5. Locations of Soil-salinity transects (red lines). Outline of Fryxell Basin indicated by cyan line. Contour interval is 50 m (thin black lines). Transects overlain on a DEM (1 m resolution) from 2014-15 LiDAR survey (Fountain et al., 2017).

SITE DESCRIPTION

The dominant hydrological features within and adjacent to MFB are alpine and piedmont glaciers that supply meltwater via transient summer streams to Lake Fryxell on the valley floor. Large expanses of bare soils and patterned ground fill in the remaining surface area and sit above a continuous layer of permafrost. MFB lies within the coastal climatic zone of the MDVs and experiences lower annual average temperatures and higher rates of precipitation than areas further inland (Obryk et al., 2020), however most snow accumulation at low elevations sublimates quickly before infiltrating adjacent soils (Chinn, 1993).

Panchromatic satellite imagery from December 5, 2011 (Figure 6) and November 25, 2018 (Figure 7) were collected to examine surface conditions for visibly wetted soils and snow on the ground during each SkyTEM survey. Visibly wetted soils were not spatially extensive and were generally limited to the wetted margins of Lake Fryxell in both 2011 and 2018. In 2011, snow near Lake Fryxell was scattered with the most prominent accumulations typically confined to stream channels. At high elevations and in locations more proximal to the coast, snow deposits were more common and more spatially extensive. Snow is visibly more widespread in the 2018 imagery but distributed similarly to 2011 with scattered snow at low elevations and more extensive accumulations at high elevations and in coastal areas of MFB.

Meteorological data from Lake Fryxell (FRLM) and Explorer's Cove (EXEM) met stations were analyzed (Figure 8) to determine the difference in stage of seasonal melt in the two years. Daily mean air temperatures at 3 m above the surface and daily mean soil temperatures at 0 cm, 5 cm, and 10 cm depth intervals were examined from the weeks

leading up to and through the AEM survey dates. In both 2011 and 2018, soil temperatures at all depth intervals are often greater than air temperatures but both tend fluctuate with each other and are related to incoming solar radiation. Soil temperatures at all depth intervals sustained daily average temperatures above 0°C during the week leading up to the 2011 AEM survey with soil temperatures at 0 cm depth exceeding 5°C at FRLM and EXEM. Soil temperatures at 5 cm and 10 cm depths also sustained temperatures above 0°C for several days prior to survey flights. On December 6, 2011, maximum daily soil temperatures (0 cm depth) reached as high as 17.4°C and 19.5°C at FRLM and EXEM, respectively. Despite soil temperatures exceeding 0°C on several days, air temperatures at FRLM did not get above 0°C until after SkyTEM flights were completed and never exceeded 0°C at EXEM.

Soil temperatures from 2018 were generally more frozen than 2011 soil temperatures for SkyTEM flight days. Soils remained frozen at all depth intervals at FRLM and EXEM through the first survey date (11/15/18) but were unfrozen during the later survey dates (11/26/18 – 11/27/18). Daily average soil temperatures (0 cm depth) from AEM survey dates peaked on 11/27/18 were 3.9°C and 4.1°C at FRLM and EXEM, respectively. Daily maximum soil temperatures (0 cm depth) between both meteorological stations were greatest on 11/26/18 at EXEM and reached a temperature of 16.1°C. Daily average soil temperatures at 5 cm depth on 11/26/18 and 11/27/18 were just above 0°C and were greater at FRLM. Soil conditions at 10 cm depth from SkyTEM flight dates were either completely frozen (11/15/18) or hovering right around freezing (11/26/18 and 11/27/18). Air temperatures at both met stations were generally lower than soil temperatures at all depths.

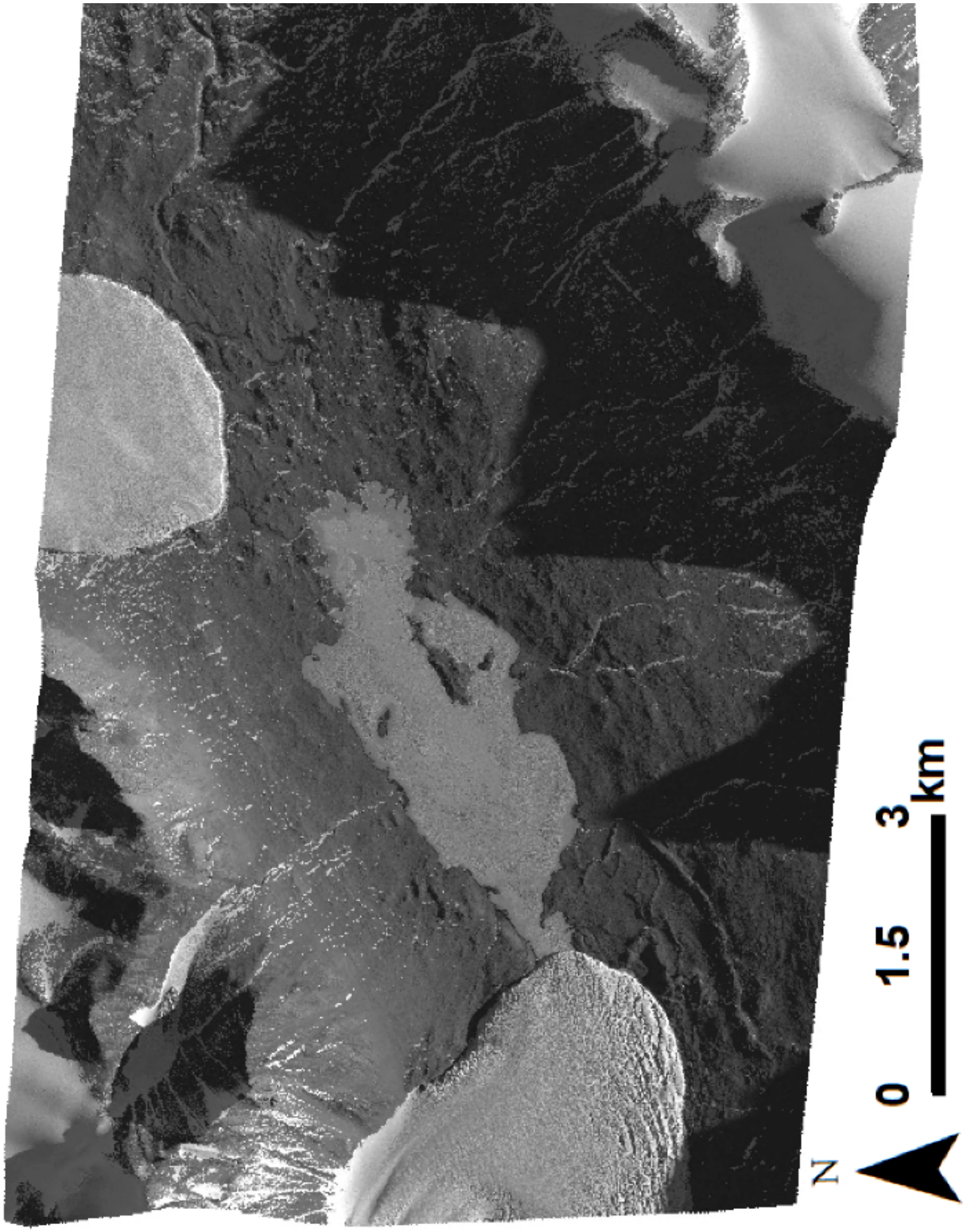

Figure 6. Quickbird 2 satellite image from December 5, 2011, over lower TV showing surface conditions during the 2011 SkyTEM resistivity survey. Brightness was increased 10% to improve visualization.

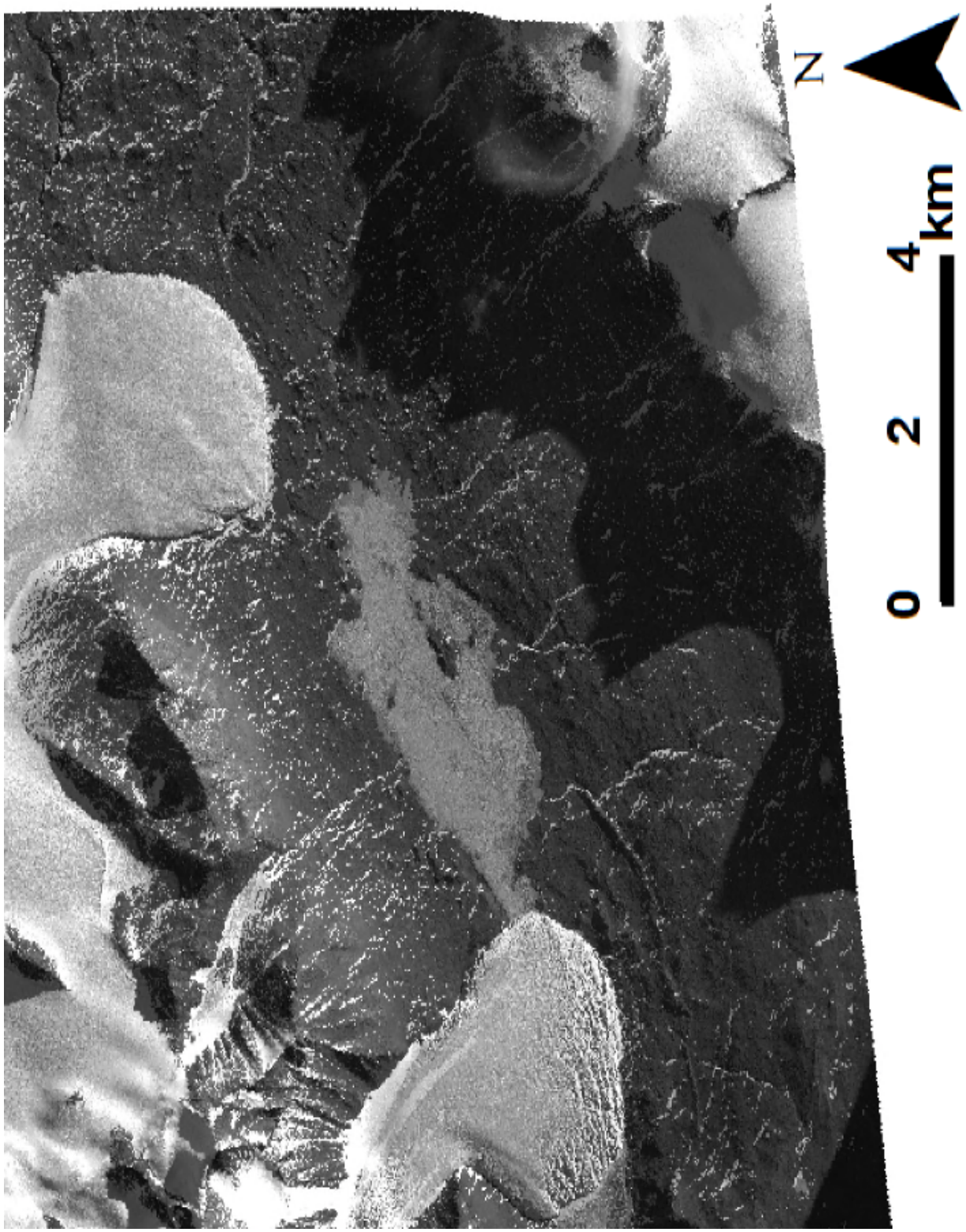

Figure 7. Worldview 3 satellite image from November 25, 2018, over Lake Fryxell showing surface conditions during the 2018 SkyTEM resistivity survey. Brightness was increased 10% to improve visualization.

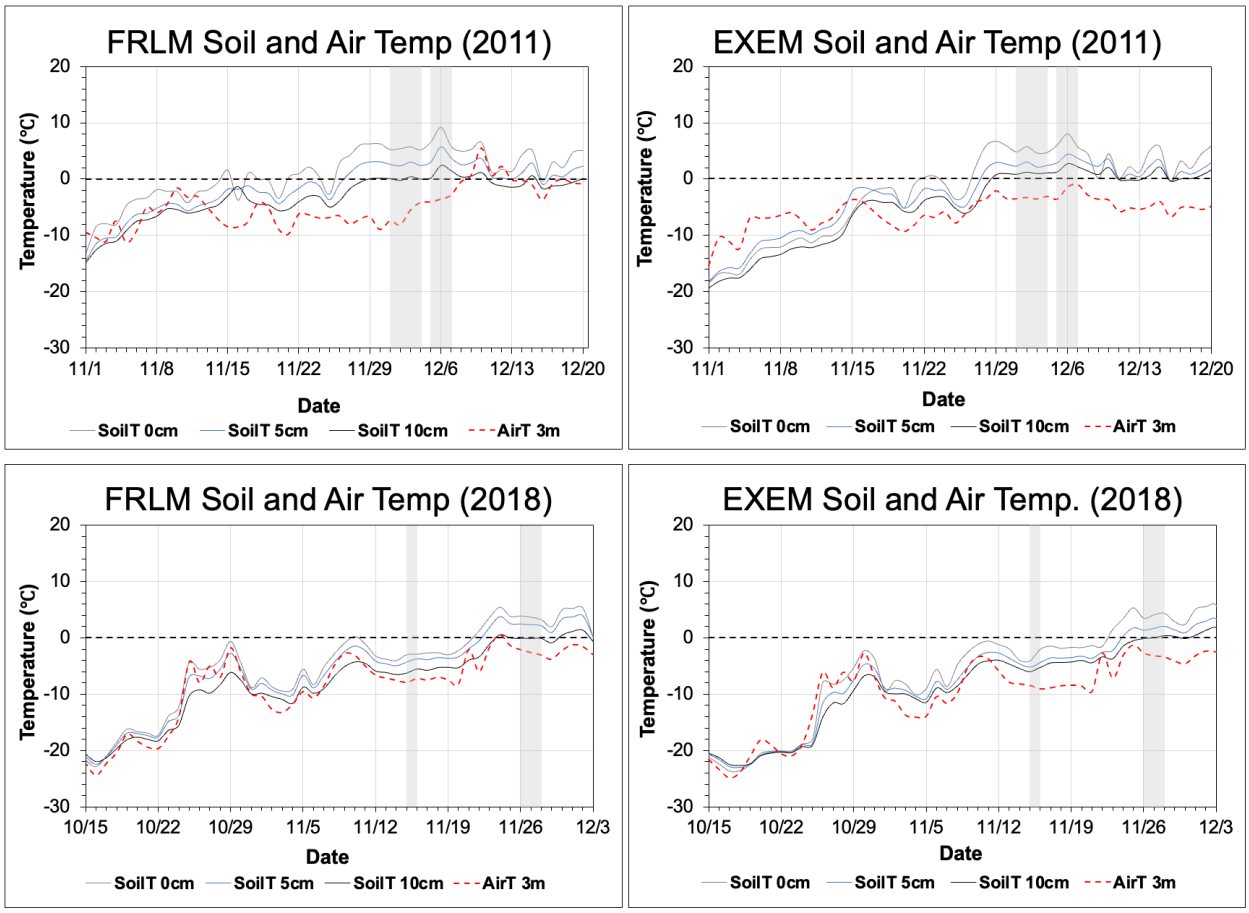

Figure 8. Air and soil temperature data (10-day moving averages) from Lake Fryxell (FRLM) and Explorer's Cove (EXEM) meteorological stations from dates leading up to and during SkyTEM resistivity surveys within the study area. SkyTEM resistivity survey dates are represented by grey shading.

RESULTS

Mean resistivity of the Fryxell Basin subsurface to 4 m was mapped from the 2011 and 2018 SkyTEM data (Figure 9). Soil resistivities are generally greater and show more variability at high elevations and tend to decrease with decreasing elevation and proximity to Lake Fryxell. An extensive zone of low resistivity (<200 Ωm; dark blue) material was detected far beyond the shorelines of Lake Fryxell and is interpreted to be sediments with elevated soil moisture contents. A second type of resistivity anomaly (~200-500 Ωm; light blue) occurs in several places near streams within MFB between ~50 masl and ~150 masl, near Delta Stream at ~250 masl, and near Huey Creek at ~50 masl (Figure 9).

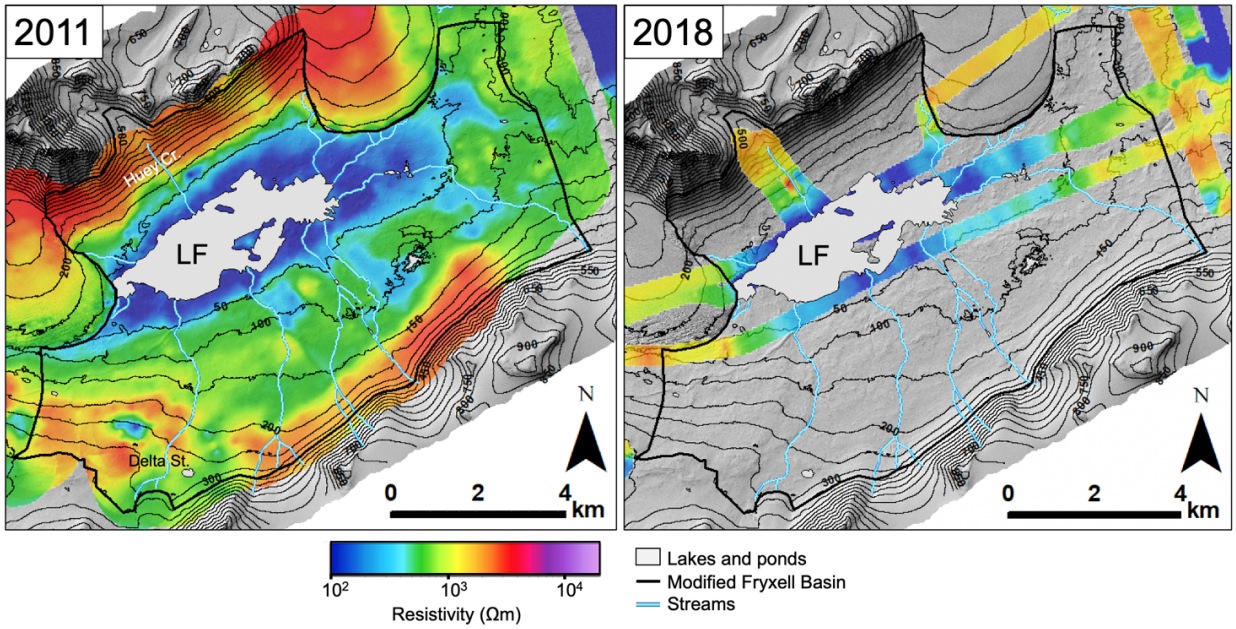

Figure 9. Mean resistivity maps of the top 4 m of the subsurface generated from the 2011 (left) and 2018 (right) SkyTEM resistivity data. A search radius of 1000 m and 250 m was used for 2011 and 2018 data interpolation, respectively. Resistivity maps are overlaid on a DEM (1 m resolution) from 2014-15 LiDAR survey (Fountain et al., 2017). Locations of Huey Creek and Delta Stream are shown in 2011 resistivity map.

Minimum and maximum resistivities range from 33.2 Ωm to 3,535 Ωm and 73.3 Ωm to 3,374 Ωm for 2011 and 2018, respectively (Figure 10; Tables 2 and 3). Soils at low

elevations (<50 masl) display the lowest resistivities in both the 2011 and 2018 AEM datasets with the average resistivity below 50 masl for 2011 and 2018 being 209.8 ± 111.4 Ωm and 282.4 ± 160.1 Ωm, respectively. Over 99% of all resistivities measured to be <200 Ωm were detected at elevations <50 masl. Average resistivities above 200 masl are an entire order of magnitude greater and display greater variability than those below 50 masl. The average elevations where <200 Ωm resistivities were detected are 27.8 ± 17.7 masl for 2011 and 20.4 ± 5.11 masl for 2018. The highest soil resistivities (>500 Ωm) detected below 50 masl are typically found near Commonwealth Glacier and Coral Ridge for both 2011 and 2018.

Table 2. 2011 SkyTEM Resistivity Statistics

Elevation (masl)	Avg. Resistivity (Ωm)	Std. Resistivity (Ωm)	Min. Resistivity (Ωm)	Max. Resistivity (Ωm)	# of Data Nodes	% of Population
<50	209.8	111.4	33.2	675.4	2034	24.8
50-100	547.6	176.3	105.4	2102	2358	28.7
100-200	834.3	428.1	247.6	3535	3272	39.8
>200	1323.5	594.2	105.5	3180	547	6.7
All	629.9	450.4	33.2	3535	8211	100

Table 3. 2018 SkyTEM Resistivity Statistics

Elevation (masl)	Avg. Resistivity (Ωm)	Std. Resistivity (Ωm)	Min. Resistivity (Ωm)	Max. Resistivity (Ωm)	# of Data Nodes	% of Population
<50	282.4	160.1	73.3	1101	382	54.1
50-100	848.1	327.5	401.9	2206	191	27.1
100-200	1028.5	217.7	601	1692	58	8.2
>200	1629.8	454.5	935.7	3374	75	10.6
All	639.9	515.9	73.3	3374	706	100

Slopes and aspects within MFB were determined to examine if either variable affected subsurface soil resistivities. High densities of measurements occurred on slopes of <5° in both the 2011 and 2018 datasets (Figure 10). Soils with resistivities <200 Ωm were detected on average slope angles of 4.8 ± 3.7° and 7.2 ± 5.9° for 2011 and 2018, respectively. High slope angles tend to be related to higher resistivity values in 2011 and 2018, however the trend seems to be more apparent in the 2018 data. Resistivities of all magnitudes occur on the full spectrum of topographic aspects in MFB and do not show any significant trends. The greatest densities occur on northern facing slopes for 2011 and for 2018 resistivities are scattered between all aspects.

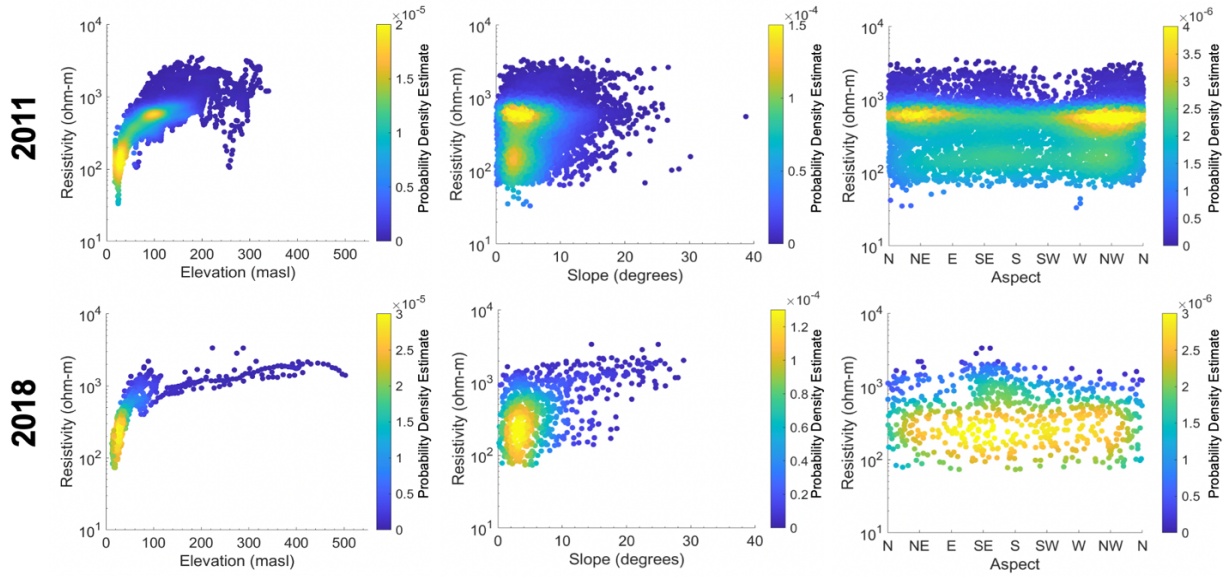

Figure 10. Data density plots of AEM resistivity variability with elevation, slope, and aspect for 2011 (top row) and 2018 (bottom row). Probability density estimates (color scale) indicate the probability that the given variables fall within a particular range of values with warm colors indicating high probability densities and cool colors indicating low probability densities. These plots show measured mean resistivity values from flight line data nodes for both SkyTEM resistivity surveys.

A resistivity difference map (Figure 11) locates areas where soil resistivity variability at locations where 2011 and 2018 resistivity maps overlap. Positive difference values represent locations where 2018 resistivities were greater than 2011 and negative

difference values show the locations where 2011 was greater. Resistivities were greater more frequently in 2018 with approximately 52% of all difference estimates producing positive values (2018 > 2011). Difference estimates ranged between -1177.5 Ωm and 2368.1 Ωm with a mean of 106.6 ± 264.9 Ωm. The range of resistivity difference

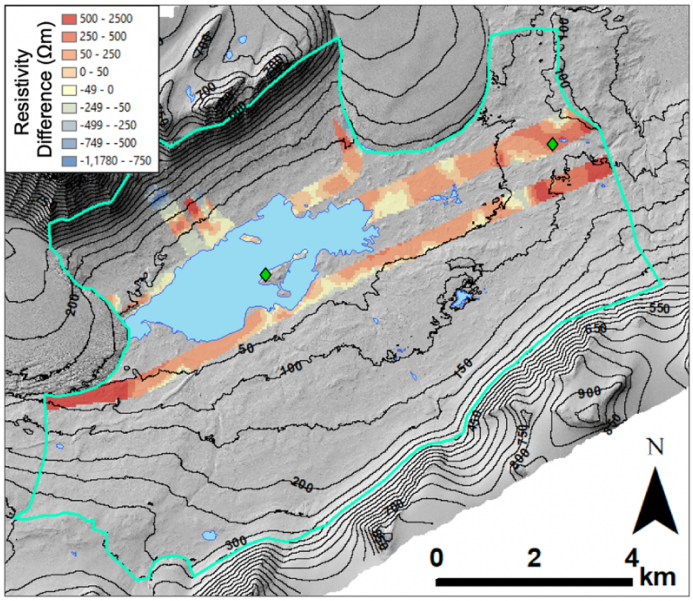

Figure 11. Resistivity difference map calculated by subtracting 2011 resistivities from 2018 resistivities where data overlap occurs. Positive (red) values indicate areas where 2018 resistivity was greater and negative (blue) areas indicate areas where 2011 resistivity was greater. Difference values are estimated using interpolated resistivity data and some degree of error is associated with all estimates. The difference in break values for the color ramp was chosen to improve resolution in low difference areas. Fryxell (FRLM) and Explorer's Cove (EXEM) met stations marked by green diamonds. Resistivity difference data is overlaid on a DEM (1 m resolution) from 2014-15 LiDAR survey (Fountain et al., 2017).

estimates below 50 masl varies between -498.7 Ωm and 1909.3 Ωm and shows less variability than higher elevations where difference estimates are typically larger in magnitude. The largest positive differences occur near the front of Canada Glacier with a maximum difference of 2368 Ωm. At elevations >125 masl difference values are primarily negative indicating greater resistivities for 2011. Negative difference estimates peak at

~190 masl with a maximum difference value of -1177.5 Ωm and then begin to move back towards zero (no difference) at higher elevations (Figure 11).

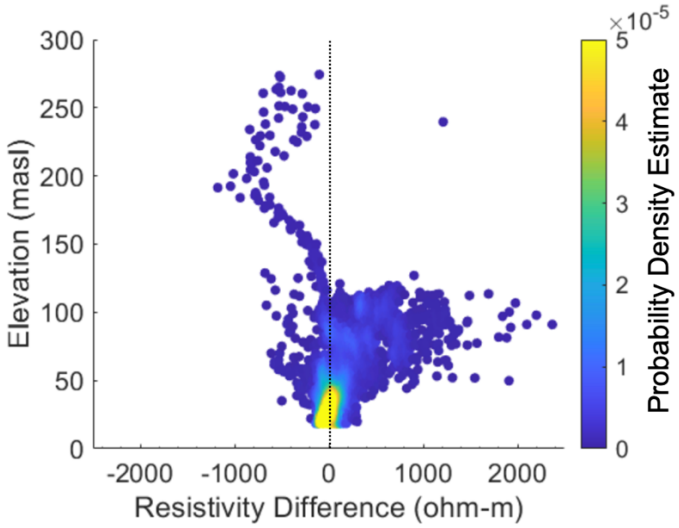

Figure 12. Resistivity differences at various elevations. Negative values indicate 2011 resistivity was greater than 2018 and positive values indicate 2018 resistivity was greater than 2011. Probability density estimates (color scale) indicate the probability that the given variables fall within a particular range of values with warm colors indicating high probability densities and cool colors indicating low probability densities.

Soil resistivities were used to calculate liquid brine fractions and generate soil moisture maps (Figure 10). A conservative cementation factor (m = 1.3, typical of unconsolidated sediments) and a brine resistivity of 8.5 Ωm were used to generate maps of liquid brine fractions. Soil moisture maps displayed similar elevational trends to soil resistivities with a clear difference in soil water contents at high and low elevations. Mean soil moisture contents below 50 masl are 10.2 ± 4.1% and 8.4 ± 3.7% for 2011 and 2018, respectively, while soils above 50 masl were drier and produced mean soil contents of 3.6 ± 1.2% and 2.7 ± 0.9% for 2011 and 2018, respectively (Figure 10). Unfrozen brine fractions can be as high 35.1% in the lowest resistivity soils and up to 8.8% in 200 Ωm soils. Estimated liquid brine contents for <200 Ωm soils range from 0.3% to 68.2% when using the values listed in Table 4 for ρ_b and m.

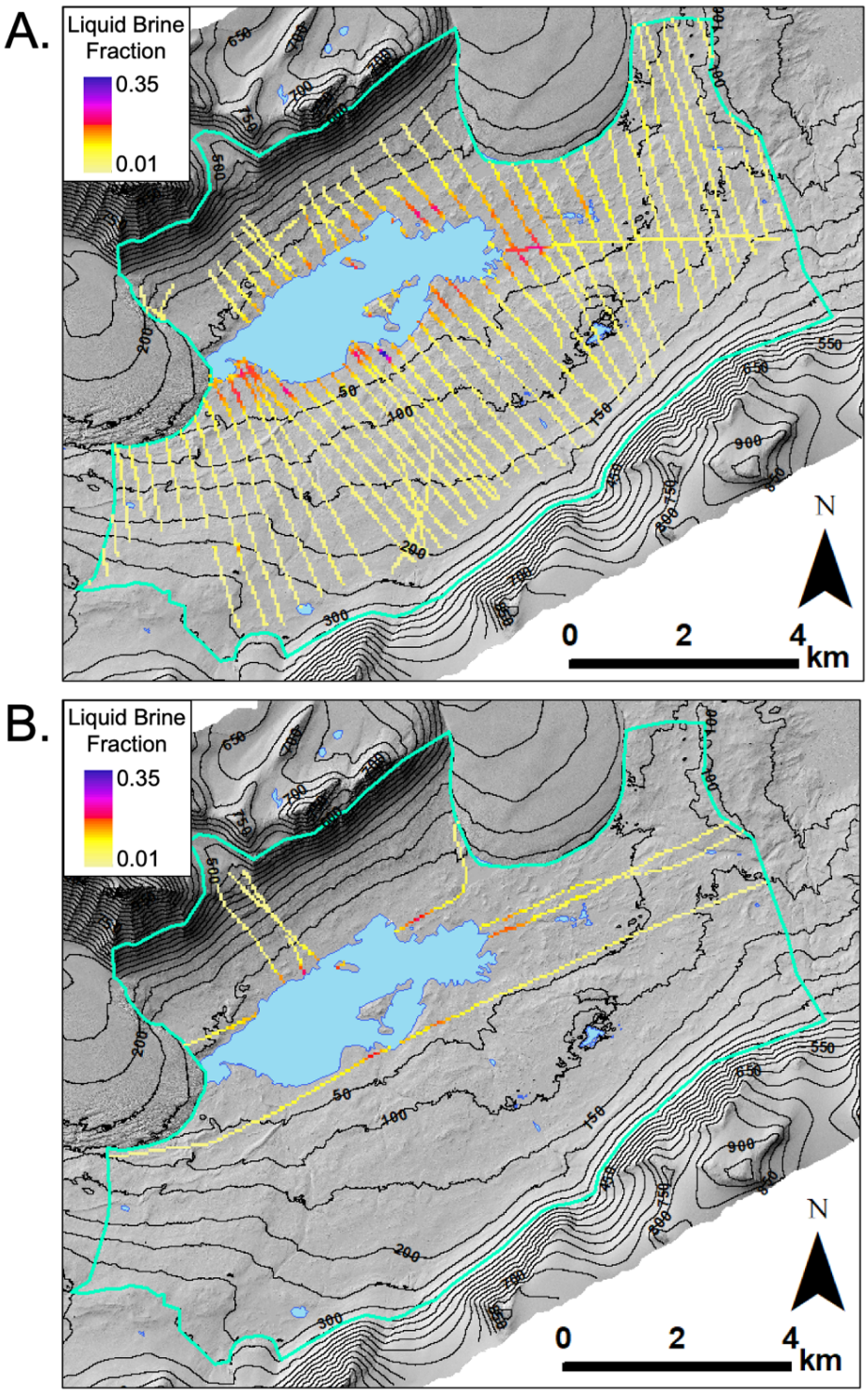

Figure 13. Map of liquid brine fractions calculated for A) 2011 and B) 2018. Both maps used ρ_b = 8.5 Ωm and m = 1.3 for Archie's Law (Archie, 1950) calculations. Contour interval is 50 m. DEM (1 m resolution) from 2014-15 LiDAR survey (Fountain et al., 2017).

Table 4. Summary of Liquid Brine Fractions (%) Calculated from AEM Resistivities. Estimated brine resistivities (ρ_b) are taken from (a) Mikucki et al., (2015) and (b) Levy et al., (2017). Bulk resistivities (ρ_0) in the top two rows are from (c) 2011 minimum soil resistivity and (d) 2018 minimum soil resistivity.

m = 1.1		**ρ_b (Ωm)**			
		18.7[b]	***8.5[a]***	***1.3[a]***	***0.36[a]***
	33.2[c]	59.3	29.0	5.3	1.6
	73.3[d]	28.9	14.1	2.6	0.8
ρ_0 (Ωm)					
	50	40.9	20.0	3.6	1.1
	100	21.8	10.6	1.9	0.6
	150	15.1	7.4	1.3	0.4
	200	11.6	5.7	1.0	0.3

m = 1.3		**ρ_b (Ωm)**			
		18.7[b]	***8.5[a]***	***1.3[a]***	***0.36[a]***
	33.2[c]	64.3	35.1	8.3	3.1
	73.3[d]	35.0	19.1	4.5	1.7
ρ_0 (Ωm)					
	50	46.9	25.6	6.0	2.2
	100	27.5	15.0	3.5	1.3
	150	20.2	11.0	2.6	1.0
	200	16.2	8.8	2.1	0.8

m = 1.5		**ρ_b (Ωm)**			
		18.7[b]	***8.5[a]***	***1.3[a]***	***0.36[a]***
	33.2[c]	68.2	40.3	11.5	4.9
	73.3[d]	40.2	23.8	6.8	2.9
ρ_0 (Ωm)					
	50	51.9	30.7	8.8	3.7
	100	32.7	19.3	5.5	2.3
	150	25.0	14.8	4.2	1.8
	200	20.6	12.2	3.5	1.5

Soil electrical conductivities (EC) from FRX-1 and interpolated SkyTEM resistivity values (extracted from the 2011 resistivity map) were plotted with corresponding percentages of silt and clay (<63 μm) (Figure 15). Soil EC showed a strong curvilinear relationship with silt and clay contents (r^2 = 0.6830; $p < 0.001$) (Figure 15a). Low percentages of fine particles were typically correlated with low soil conductivities and all

samples with silt and clay percentages exceeding 10% displayed elevated conductivities between 287 µS/cm and 5970 µS/cm. SkyTEM resistivities displayed a similar relationship to the percentage of fine particles (r^2 = 0.401; p < 0.001) (Figure15b). Soil resistivities increase rapidly in soils with silt and clay percentages >10%. The mean soil resistivity where fine-grained particles were >10% was 367.2 ± 46.2 Ωm, which is far less than soils with <10% fines (mean = 1859.8 ± 1065.0 Ωm).

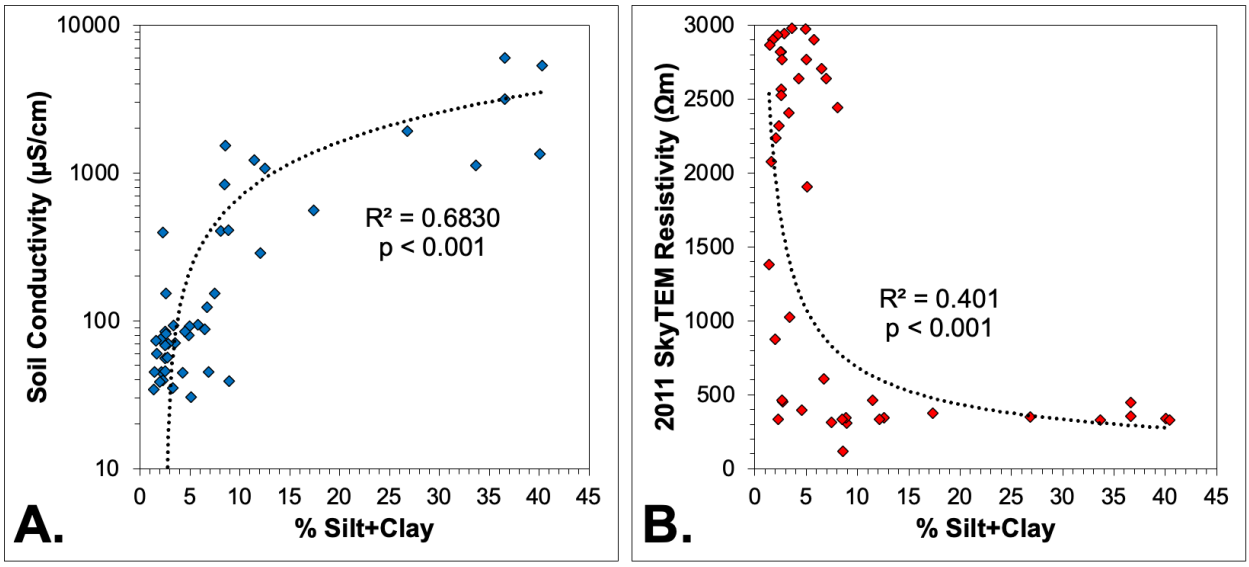

Figure 14. A) Soil conductivity and B) SkyTEM resistivity values extracted from FRX-1 plotted with percentage of silt and clay. Figure 14a shows a curvilinear line fit and Figure14b uses a power line fit. The location of FRX-1 is shown in Figure 5.

Soil properties along three transects were analyzed and compared to AEM resistivity data to determine if soil properties displayed similar spatial trends. EC measurements from all three transects showed that soil EC typically peaks between ~50 masl and ~100 masl (Figure 14). Maximum EC values were 5970 µS/cm, 12830 µS/cm, and 20000 µS/cm for FRX-1, FRX-2, and FRX-3, respectively. The average conductivity from all FRX-3 EC measurements is an order of magnitude greater than those of FRX-1 and FRX-2. In FRX-1 and FRX-2 there is a noticeable increase in EC values below 100

masl, while FRX-3 shows a similar increase in EC below 140 masl. Average EC values below 100 masl were two orders of magnitude greater than those above 100 masl for FRX-1 and one order of magnitude greater for FRX-2 while FRX-3 showed high EC variability above and below 150 masl.

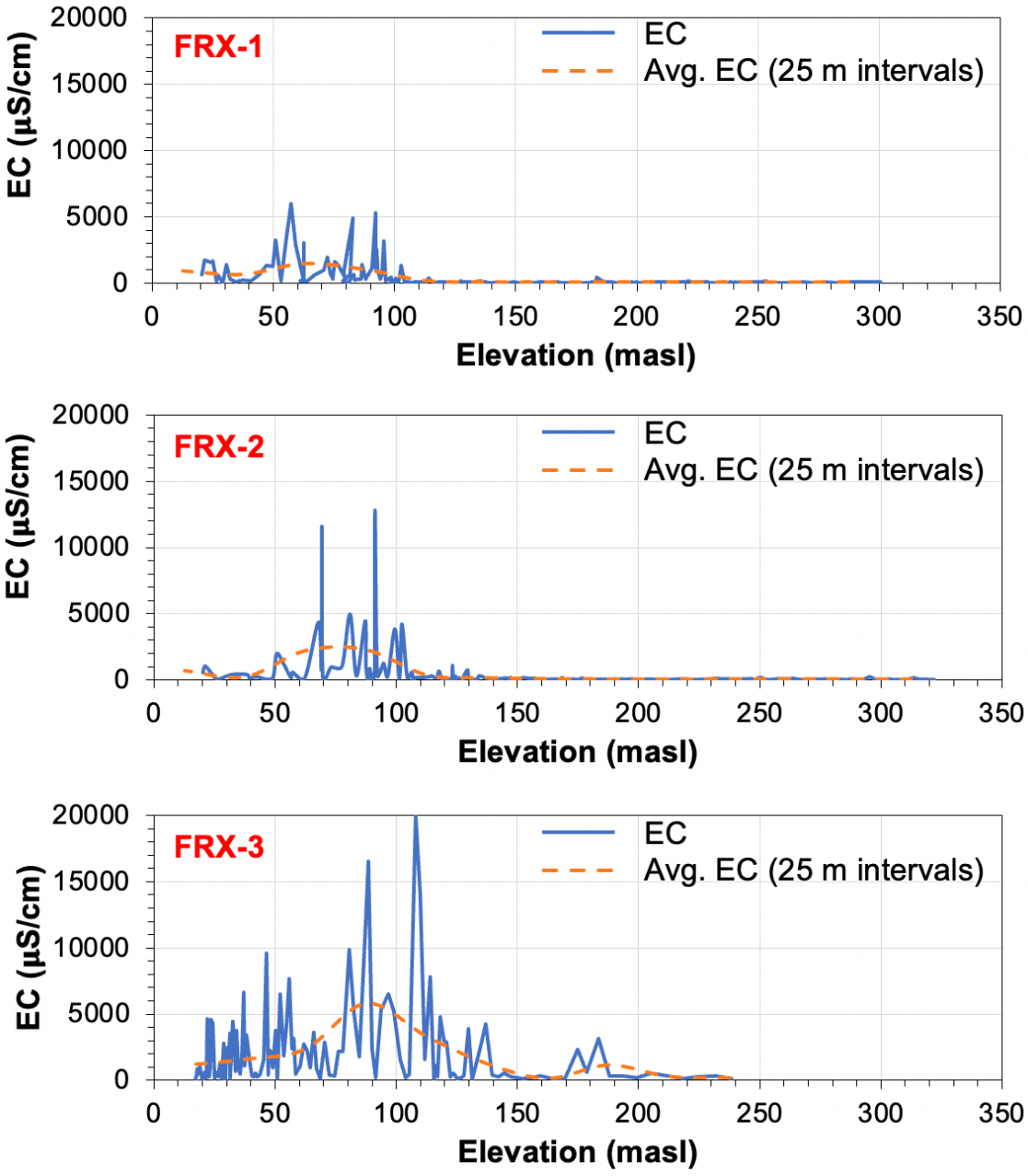

Figure 15. Electrical conductivities at varying elevations from soil samples collected along soil-salinity transects (FRX 1-3). Transect locations shown in Figure 5.

DISCUSSION

Soil properties in lower TV are spatially heterogenous in the shallow subsurface and are affected by a combination of site history, local and regional climate, proximity to water sources, ice/water content, and depth (Ugolini et al., 1981; Levy and Schmidt, 2016; Wlostowski et al., 2017). Shallow subsurface (<4 m depth) resistivities detected during two SkyTEM resistivity surveys from 2011 and 2018 were analyzed to provide novel insight into the controls on spatial variability of soil geochemical properties in the near subsurface of Fryxell Basin.

Resistivities in the top 4 m (2011 and 2018) of the MFB subsurface display highly variable conditions at high and low elevations. Soil resistivities roughly align with the topography of the landscape with low resistivity soils primarily occurring at low elevations near Lake Fryxell and high resistivity soils dominating higher elevations and the coastal portions of MFB (Figure 9). The large contrast in electrical resistivity at high and low elevations is predominantly due to relatively large differences in soil moisture content at the time of each SkyTEM survey. Frozen soil water can increase electrical resistivity values by several orders of magnitude (Hoekstra and McNeill, 1973), which allows resistivity to be used as a proxy for the temperature and soil moisture content of near surface sediments. In high elevation and coastal soils, the depth to the ice table is small (Bockheim et al., 2007) and soil moisture contents are typically very low (Campbell et al., 2013) and high soil resistivities in these areas frequently displayed similarly dry and/or frozen conditions (Figure 13). Low elevation soils proximal to Lake Fryxell were typically characterized by low resistivities indicating warmer soil temperatures and elevated soil moisture contents. An extensive zone of low resistivity material (<200 Ωm) was detected

stretching far beyond the shore of Lake Fryxell and is interpreted to be sediments partially saturated with unfrozen brine (Figure 13). Soil moisture is the primary factor controlling thermal properties, such as thermal diffusivity (i.e., the soil's ability to transfer heat to colder surrounding materials), in active layer soils, which affects permafrost thaw rates at the ice-table interface (Levy and Schmidt, 2016).

Partially saturated soils (<200 Ωm) are predominantly found at elevations <50 masl where paleolake highstands (evidenced by high elevation paleodeltas) would have promoted the deposition of fine-grained sediments affecting soil compositions at these elevations. Three soil geochemical transects show a noticeable transition from low soil conductivities at high elevations to high soil conductivities at lower elevations, although this transition happens at slightly different elevations (~100 masl to ~140 masl) in each transect (Figure 15). Elevated soil conductivities are related to increased fine-grained particles at these elevations as evidenced by particle size data from FRX-1 (Figure 14a). SkyTEM resistivity values extracted along FRX-1 show a significant correlation to silt and clay fractions where low resistivities are typically associated with elevated fine-grained particle contents (Figure 14b). The data show that SkyTEM resistivities are highest when silt and clay percentages are <10%. Soils with greater percentages of fine-grained particles have higher porosities and more capillary lift than coarser soils due to smaller pore diameters. This allows finer-grained soils at low elevations to hold more water and solutes in place than coarser sediments where liquids and salts could be easily flushed out (Ugolini et al., 1981). Additionally, fine-grained sediments typically display salinities up to 10 times greater than coarser sediments in the MDVs (Ugolini et al., 1981). Soil pore water interacting with the fine-grained minerals soils at low elevations would promote

the leeching of solutes into the soil column, ultimately increasing soil and brine salinities and driving resistivity signals down.

At elevations >50 masl, soil resistivities display higher variability and begin to rapidly increase in magnitude with increasing elevation (Figures 9 and 10, Tables 2 and 3). High elevation soils with high resistivities (>500 Ωm) are characterized as having very low soil moisture contents (Figure 13) and are likely frozen at the highest elevations within MFB. At these elevations, ice-cemented and dry-frozen permafrost are very common in the near subsurface and active layers are thin to non-existent (Bockheim et al., 2007). This indicates that most of the high resistivity signals above 50 masl are primarily due to coarser sediments sitting above frozen permafrost. However, several anomalous zones of relatively lower resistivities (200 Ωm to 500 Ωm) exist between 50 and 150 masl near stream channels. These areas display higher resistivities than the threshold for brine saturated sediments (<200 Ωm) while also showing visibly lower resistivities than the surrounding sediments, indicating the presence of thermally degrading ice-cored sediments and greater soil water contents.

Resistivity variability between locations that overlap in the 2011 and 2018 SkyTEM surveys are primarily due to differences in local climate conditions at the time of each survey. It is highly unlikely that there were any significant changes in soil lithology composition during the relatively short time span between SkyTEM surveys (~7 years), indicating soil moisture contents varied at similar locations due to differences in soil temperatures in 2011 and 2018. Although the 2018 SkyTEM survey is far less spatially extensive, resistivities in 2018 typically were greater than 2011 resistivities (Figures 11 and 12, Tables 2 and 3) reflecting the colder soil temperatures observed at FRLM and

EXEM during the 2018 survey in MFB (Figure 8). Daily average soil temperatures in 2011 remained above 0°C for several days leading up to and throughout the duration of the 2011 SkyTEM survey in MFB, while 2018 soil temperature did not get above freezing until after the first SkyTEM flights on 11/15/18. Elevated soil temperatures, especially at increased depths, can generate soil moisture from pore-ice and permafrost leading to an increase in the soil water contents at low elevations soils where fine-grained sediments are found in greater abundance. Elevated soil moisture contents are the primary cause of low resistivities in low elevation soils within MFB. Additionally, the leaching of solutes from minerals interacting with the soil water would increase the salinity and decrease the resistivity of the formation.

CONCLUSIONS

Electrical resistivities mapped from 2011 and 2018 SkyTEM surveys provide a detailed look into the hydrological structure of the shallow subsurface (top 4 m) in lower TV. Soil resistivities ranged from 33.2 Ωm to 3535 Ωm and displayed highly heterogenous conditions over short (meter-scale) and long (kilometer-scale) distances. Low resistivity (<200 Ωm) soils are most common below 50 masl and are interpreted to contain soil moisture contents between 0.3% and 68.2%. High resistivity (>200 Ωm) soils dominate at high elevations and are characterized as frozen soils overlying permafrost (i.e., ice-cemented or dry-frozen). Grain size distribution from FRX-1 indicate an increase in fine-grained (<63 μm) sediments below ~100 masl, which leads to increased soil porosities and greater capillary attraction that promote increases in soil moisture at low elevations. Soil resistivities observed in this study are ultimately the product of local and regional climate variability, site history, and topography that characterize lower TV.

Soil geochemical properties are highly heterogeneous in the shallow subsurface of lower TV and differ at high and low elevations primarily due to differences in soil moisture contents, which is controlled by local climate conditions. As solar radiation and air temperatures continue to increase in the MDVs (Obryk et al., 2020), the hydrological connectivity across the landscape will likely increase (Gooseff et al., 2017) and soil attributes will reflect these changing conditions.

REFERENCES

Archie, G.E., 1942, The Electrical Resistivity Log as an Aid in Determining Some Reservoir Characteristics: Transactions of the AIME, v. 146, no. 01, p. 54–62, doi: 10.2118/942054-g.

Archie, G.E., 1950, Introduction to Petrophysics of Reservoir Rocks: AAPG Bulletin, v. 34, doi: 10.1306/3d933f62-16b1-11d7-8645000102c1865d.

Auken, E., Christiansen, A.V., Westergaard, J.H., Kirkegaard, C., Foged, N., and Viezzoli, A., 2009, An integrated processing scheme for high-resolution airborne electromagnetic surveys, the SkyTEM system: Exploration Geophysics, v. 40, no. 2, p. 184–192, doi: 10.1071/eg08128.

Barrett, J.E., Gooseff, M.N., and Takacs-Vesbach, C., 2009, Spatial variation in soil active-layer geochemistry across hydrologic margins in polar desert ecosystems: Hydrology and Earth System Sciences, v. 13, no. 12, p. 2349–2358, doi: 10.5194/hess-13-2349-2009.

Bindschadler, R., Vornberger, P., Fleming, A., Fox, A., Mullins, J., Binnie, D., Paulsen, S., Granneman, B., and Gorodetzky, D., 2008, The Landsat Image Mosaic of Antarctica: Remote Sensing of Environment, v. 112, no. 12, p. 4214–4226, doi: 10.1016/j.rse.2008.07.006.

Bockheim, J.G., 2002, Landform and Soil Development in the McMurdo Dry Valleys, Antarctica: A Regional Synthesis: Arctic, Antarctic, and Alpine Research, v. 34, no. 3, p. 308, doi: 10.2307/1552489.

Bockheim, J.G., and McLeod, M., 2008, Soil distribution in the McMurdo Dry Valleys, Antarctica: Geoderma, v. 144, no. 1-2, p. 43–49, doi: 10.1016/j.geoderma.2007.10.015.

Bockheim, J.G., Campbell, I.B., and McLeod, M., 2007, Permafrost distribution and active-layer depths in the McMurdo Dry Valleys, Antarctica: Permafrost and Periglacial Processes, v. 18, no. 3, p. 217–227, doi: 10.1002/ppp.588.

Byun, Y.-H., Hong, W.-T., and Yoon, H.-K., 2019, Characterization of Cementation Factor of Unconsolidated Granular Materials Through Time Domain Reflectometry with Variable Saturated Conditions: Materials, v. 12, no. 8, p. 1340, doi: 10.3390/ma12081340.

Campbell, I.B., Claridge, G.G., Campbell, D.I., and Balks, M.R., 2013, The Soil Environment of the Mcmurdo Dry Valleys, Antarctica: Ecosystem Dynamics in a Polar Desert: the Mcmurdo Dry Valleys, Antarctica, p. 297–322, doi: 10.1029/ar072p0297.

Cartwright, K., and Harris, H.J., 1981, Hydrogeology of the dry valley region, Antarctica: Dry Valley Drilling Project, p. 193–214, doi: 10.1029/ar033p0193.

Chinn, T.J., 1993, Physical and Biogeochemical Processes in Antarctic Lakes: AGU Journals.

Chinn, T.J., 1990, The Dry Valleys in Antarctica: the Ross Sea Region: Department of Scientific and Industrial Research: Wellington,. NZ, p. 137–153.

Decker, E.R., and Bucher, G.J., 1982, Geothermal studies in the Ross Island- Dry Valley region: Antarctic geoscience: The University of Wisconsin Press, p. 887–894.

Foley, N., Tulaczyk, S., Auken, E., Schamper, C., Dugan, H., Mikucki, J., Virginia, R., and Doran, P., 2016, Helicopter-borne transient electromagnetics in high-latitude environments: An application in the McMurdo Dry Valleys, Antarctica: GEOPHYSICS, v. 81, no. 1, doi: 10.1190/geo2015-0186.1.

Foley, N., Tulaczyk, S.M., Grombacher, D., Doran, P.T., Mikucki, J., Myers, K.F., Foged, N., Dugan, H., Auken, E., and Virginia, R., 2019, Evidence for Pathways of Concentrated Submarine Groundwater Discharge in East Antarctica from Helicopter-Borne Electrical Resistivity Measurements: Hydrology, v. 6, no. 2, p. 54, doi: 10.3390/hydrology6020054.

Fountain, A.G., Fernandez-Diaz, J.C., Obryk, M., Levy, J., Gooseff, M., Van Horn, D.J., Morin, P., and Shrestha, R., 2017, High-resolution elevation mapping of the McMurdo Dry Valleys, Antarctica, and surrounding regions: Earth System Science Data, v. 9, no. 2, p. 435–443, doi: 10.5194/essd-9-435-2017.

Fountain, A.G., Nylen, T.H., Monaghan, A., Basagic, H.J., and Bromwich, D., 2009, Snow in the McMurdo Dry Valleys, Antarctica: International Journal of Climatology, v. 30, no. 5, p. 633–642, doi: 10.1002/joc.1933.

Frohlich, R.K., and Parke, C.D., 1989, The Electrical Resistivity of the Vadose Zone - Field Survey: Ground Water, v. 27, no. 4, p. 524–530, doi: 10.1111/j.1745-6584.1989.tb01973.x.

Gooseff, M.N., Barrett, J.E., Adams, B.J., Doran, P.T., Fountain, A.G., Lyons, W.B., McKnight, D.M., Priscu, J.C., Sokol, E.R., Takacs-Vesbach, C., Vandegehuchte, M.L., Virginia, R.A., and Wall, D.H., 2017, Decadal ecosystem response to an anomalous melt season in a polar desert in Antarctica: Nature Ecology & Evolution, v. 1, no. 9, p. 1334–1338, doi: 10.1038/s41559-017-0253-0.

Gooseff, M.N., Barrett, J.E., and Levy, J.S., 2013, Shallow groundwater systems in a polar desert, McMurdo Dry Valleys, Antarctica: Hydrogeology Journal, v. 21, no. 1, p. 171–183, doi: 10.1007/s10040-012-0926-3.

Gooseff, M.N., Barrett, J.E., Doran, P.T., Fountain, A.G., Lyons, W.B., Parsons, A.N., Porazinska, D.L., Virginia, R.A., and Wall, D.H., 2003, Snow-Patch Influence on Soil Biogeochemical Processes and Invertebrate Distribution in the McMurdo Dry Valleys, Antarctica: Arctic, Antarctic, and Alpine Research, v. 35, no. 1, p. 91–99, doi: 10.1657/1523-0430(2003)035[0091:spiosb]2.0.co;2.

Gooseff, M.N., Barrett, J.E., Northcott, M.L., Bate, D.B., Hill, K.R., Zeglin, L.H., Bobb, M., and Takacs-Vesbach, C.D., 2007, Controls on the Spatial Dimensions of Wetted Hydrologic Margins of Two Antarctic Lakes: Vadose Zone Journal, v. 6, no. 4, p. 841–848, doi: 10.2136/vzj2006.0161.

Gooseff, M.N., McKnight, D.M., Doran, P., Fountain, A.G., and Lyons, W.B., 2011, Hydrological Connectivity of the Landscape of the McMurdo Dry Valleys, Antarctica: Geography Compass, v. 5, no. 9, p. 666–681, doi: 10.1111/j.1749-8198.2011.00445.x.

Hoekstra, P., and McNeill, D., 1973, in 2nd Int. Conf. Permafrost. 2, 517–526 (Yakutsk,Russia, 1973).

Hoffman, M.J., Fountain, A.G., and Liston, G.E., 2016, Distributed modeling of ablation (1996–2011) and climate sensitivity on the glaciers of Taylor Valley, Antarctica: Journal of Glaciology, v. 62, no. 232, p. 215–229, doi: 10.1017/jog.2015.2.

Ikard, S.J., Gooseff, M.N., Barrett, J.E., and Takacs-Vesbach, C., 2009, Thermal characterisation of active layer across a soil moisture gradient in the McMurdo Dry Valleys, Antarctica: Permafrost and Periglacial Processes, v. 20, no. 1, p. 27–39, doi: 10.1002/ppp.634.

Levy, J., 2012, How big are the McMurdo Dry Valleys? Estimating ice-free area using Landsat image data: Antarctic Science, v. 25, no. 1, p. 119–120, doi: 10.1017/s0954102012000727.

Levy, J.S., and Schmidt, L.M., 2016, Thermal properties of Antarctic soils: wetting controls subsurface thermal state: Antarctic Science, v. 28, no. 5, p. 361–370, doi: 10.1017/s0954102016000201.

Levy, J., Fountain, A., Lyons, W.B., and Welch, K., 2014, Experimental formation of pore fluids in McMurdo Dry Valleys soils: Antarctic Science, v. 27, no. 2, p. 163–171, doi: 10.1017/s0954102014000479.

Levy, J.S., Fountain, A.G., Gooseff, M.N., Welch, K.A., and Lyons, W.B., 2011, Water tracks and permafrost in Taylor Valley, Antarctica: Extensive and shallow groundwater connectivity in a cold desert ecosystem: Geological Society of America Bulletin, v. 123, no. 11-12, p. 2295–2311, doi: 10.1130/b30436.1.

Levy, J.S., Fountain, A.G., Obryk, M.K., Telling, J., Glennie, C., Pettersson, R., Gooseff, M., and Van Horn, D.J., 2018, Decadal topographic change in the McMurdo Dry Valleys of Antarctica: Thermokarst subsidence, glacier thinning, and transfer of water storage from the cryosphere to the hydrosphere: Geomorphology, v. 323, p. 80–97, doi: 10.1016/j.geomorph.2018.09.012.

McGinnis, L.D., and Jensen, T.E., 1971, Permafrost-Hydrogeologic Regimen in Two Ice-Free Valleys, Antarctica, from Electrical Depth Sounding: Quaternary Research, v. 1, no. 3, p. 389–409, doi: 10.1016/0033-5894(71)90073-1.

McKay, C.P., Mellon, M.T., and Friedmann, E.I., 1998, Soil temperatures and stability of ice-cemented ground in the McMurdo Dry Valleys, Antarctica: Antarctic Science, v. 10, no. 1, p. 31–38, doi: 10.1017/s0954102098000054.

McKelvey, B.C., 1981, The lithologic logs of DVDP cores 10 And 11, Eastern Taylor Valley: Dry Valley Drilling Project, p. 63–94, doi: 10.1029/ar033p0063.

Mikucki, J.A., Auken, E., Tulaczyk, S., Virginia, R.A., Schamper, C., Sørensen, K.I., Doran, P.T., Dugan, H., and Foley, N., 2015, Deep groundwater and potential subsurface habitats beneath an Antarctic dry valley: Nature Communications, v. 6, no. 1, doi: 10.1038/ncomms7831.

Obryk, M.K., Doran, P.T., Fountain, A.G., Myers, M., and McKay, C.P., 2020, Climate From the McMurdo Dry Valleys, Antarctica, 1986–2017: Surface Air Temperature Trends and Redefined Summer Season: Journal of Geophysical Research: Atmospheres, v. 125, no. 13, doi: 10.1029/2019jd032180.

Prentice, M.L., Kleman, J.L., and Stroeven, A.P., 2013, The Composite Glacial Erosional Landscape of the Northern Mcmurdo Dry Valleys: Implications for Antarctic Tertiary Glacial History: Ecosystem Dynamics in a Polar Desert: the Mcmurdo Dry Valleys, Antarctica, p. 1–38, doi: 10.1029/ar072p0001.

Schmidt, L.M., and Levy, J.S., 2017, Hydraulic conductivity of active layer soils in the McMurdo Dry Valleys, Antarctica: Geological legacy controls modern hillslope connectivity: Geomorphology, v. 283, p. 61–71, doi: 10.1016/j.geomorph.2017.01.038.

Toner, J.D., and Sletten, R.S., 2013, The formation of Ca-Cl-rich groundwaters in the Dry Valleys of Antarctica: Field measurements and modeling of reactive transport: Geochimica et Cosmochimica Acta, v. 110, p. 84–105, doi: 10.1016/j.gca.2013.02.013.

Ugolini, F.C., and Anderson, D.M., 1973, Ionic Migration and Weathering in Frozen Antarctic Soils: Soil Science, v. 115, no. 6, p. 461–470, doi: 10.1097/00010694-197306000-00010.

Ugolini, F.C., Deutsch, W., and Harris, H.J., 1981, Chemistry and clay mineralogy of selected cores from the Antarctic Dry Valley Drilling Project: Dry Valley Drilling Project, p. 315–329, doi: 10.1029/ar033p0315.

Ward, S.H., and Hohmann, G.W., 1988, Electromagnetic Theory for Geophysical Applications: Electromagnetic Methods in Applied Geophysics, p. 130–311, doi: 10.1190/1.9781560802631.ch4.

Wlostowski, A.N., Gooseff, M.N., and Adams, B.J., 2018, Soil Moisture Controls the Thermal Habitat of Active Layer Soils in the McMurdo Dry Valleys, Antarctica: Journal of Geophysical Research: Biogeosciences, v. 123, no. 1, p. 46–59, doi: 10.1002/2017jg004018.

VITA

William Scott Gutterman received his bachelor's degree from the University of Colorado at Boulder in 2017 and he will receive his master's degree from Louisiana State University in August of 2021. He was introduced to research in the geosciences as an undergraduate where he studied sedimentary basins to characterize petroleum systems, but his interests also included hydrogeology. An opportunity to study Antarctic soils as a master's student confirmed his passion for the Earth Sciences. Upon completion of his master's degree, William plans to start a career in the geosciences, and he hopes to contribute to environmental research whenever possible.